ARTICLE

OPEN

Check for updates

Surprisingly long lifetime of methacrolein oxide, an isoprene derived Criegee intermediate, under humid conditions

Yen-Hsiu Lin[1], Cangtao Yin [1], Kaito Takahashi [1] & Jim Jr-Min Lin [1,2✉]

Ozonolysis of isoprene, the most abundant alkene, produces three distinct Criegee intermediates (CIs): CH_2OO, methyl vinyl ketone oxide (MVKO) and methacrolein oxide (MACRO). The oxidation of SO_2 by CIs is a potential source of H_2SO_4, an important precursor of aerosols. Here we investigated the UV-visible spectroscopy and reaction kinetics of thermalized MACRO. An extremely fast reaction of *anti*-MACRO with SO_2 has been found, $k_{SO2} = (1.5 \pm 0.4) \times 10^{-10} \ cm^3 \ s^{-1}$ ($\pm 1\sigma$, σ is the standard deviation of the data) at 298 K (150 − 500 Torr), which is ca. 4 times the value for *syn*-MVKO. However, the reaction of *anti*-MACRO with water vapor has been observed to be quite slow with an effective rate coefficient of $(9 \pm 5) \times 10^{-17} \ cm^3 \ s^{-1}$ ($\pm 1\sigma$) at 298 K (300 to 500 Torr), which is smaller than current literature values by 1 or 2 orders of magnitude. Our results indicate that *anti*-MACRO has an atmospheric lifetime (best estimate ca. 18 ms at 298 K and RH = 70%) much longer than previously thought (ca. 0.3 or 3 ms), resulting in a much higher steady-state concentration. Owing to larger reaction rate coefficient, the impact of *anti*-MACRO on the oxidation of atmospheric SO_2 would be substantial, even more than that of *syn*-MVKO.

[1] Institute of Atomic and Molecular Sciences, Academia Sinica, Taipei, Taiwan. [2] Department of Chemistry, National Taiwan University, Taipei, Taiwan. ✉email: jimlin@gate.sinica.edu.tw

soprene is the most abundant unsaturated hydrocarbon in the atmosphere[1]. Ozonolysis of isoprene produces three kinds of carbonyl oxides (also called Criegee Intermediates, CIs): CH_2OO, methyl vinyl ketone oxide (MVKO: $CH_3C(C_2H_3)OO$), and methacrolein oxide (MACRO: $CH_2=C(CH_3)CHOO$)[2–4]. CIs are very reactive species. In 2012, their reactions with SO_2 were found to be faster than previously thought by orders of magnitude[5]. The oxidation of SO_2 ($SO_2 \rightarrow SO_3$) has gained wide attention because it is an important process in the formation of secondary aerosols ($SO_3 \rightarrow H_2SO_4$)[6–15]. Field and chamber studies, pioneered by Mauldin et al.[9], indicate that there is a non-OH oxidant contributing to the oxidation of atmospheric SO_2 and this new oxidant may be Criegee intermediates[9–15]. However, it is impractical to measure the very reactive CIs in the atmosphere. Their atmospheric concentrations can only be estimated through kinetics analysis. For example, Novelli et al. have given an average estimate of the CI concentration of ca. 5×10^4 molecules cm^{-3} (with an order of magnitude uncertainty) for the two environments they studied[16]. (For simplicity, we will use 'cm^{-3}' for the unit of molecular number density, instead of the more formal 'molecules cm^{-3}'.) Note that older estimations may have larger uncertainties in the CI concentrations since the related reaction kinetics were not well determined at that time.

On the other hand, laboratory studies on individual CI reactions have revealed that the reactivity (thus the atmospheric fate) of a CI would strongly depend on its structure[17,18]. For CH_2OO and $anti$-CH_3CHOO, which have a H-atom at the syn position, the main decay pathway is their reactions with water vapor (H_2O monomer and dimer)[18–23]. These reactions are extremely fast, resulting in very low steady-state concentrations of such CIs, which are too low to oxidize atmospheric SO_2 at any substantial level[17]. For syn-CH_3CHOO and $(CH_3)_2COO$, which have an alkyl group at the syn position, their unimolecular reactions via intramolecular 1,4-H-atom transfer are the major decay process, which also generates OH radicals[24–31]. These unimolecular processes are not slow and essentially limit the steady-state concentrations of such CIs[17,32].

Different from alkyl-substituted CIs, MVKO and MACRO have a C=C double bond, which forms extended conjugation with the carbonyl oxide functional group (resonance stabilized). The pioneering works of Lester and coworkers have demonstrated a photolytic synthesis method that allows direct detection of MVKO and MACRO[33,34]. Via this new synthesis scheme, recent studies have shown that the resonance-stabilization would affect the reactivity and thus the atmospheric fate of MVKO[35,36].

For MVKO, there are four possible isomers (or conformers)[2,33,35,37]. Similar to simpler CIs, the barrier of rotating the carbonyl C=O bond is high, resulting in non-interconverting syn and $anti$ isomers (following the nomenclature of Barbar et al.)[33,38]. However, the barrier of rotating the C—C single bond between the C=C and C=O bonds is low, giving essentially an equilibrium mixture of cis and $trans$ conformers[32,39,40]. It has been predicted that $anti$-$trans$-MVKO would quickly interconvert to $anti$-cis-MVKO ($>10^6 s^{-1}$)[32], which decays quickly via fast 1,5-ring closure to form dioxole with a rate coefficient of ca. $2100 s^{-1}$ at 298 K[32,33,41,42]. As a result, $anti$-MVKO was not observed experimentally, presumably due to short lifetime and/or low yield[35].

Caravan et al. have found that syn-MVKO reacts with SO_2 and formic acid as fast as other alkyl CIs do. Furthermore, based on their global chemistry and transport model, they have shown that syn-MVKO could significantly increase the atmospheric oxidation of SO_2 and the removal of formic acid, where the isoprene emission is high. The high impact of syn-MVKO is mostly due to the abundance of isoprene (its source) and its slow decay (slow unimolecular decay and slow reaction with water vapor)[35]. The

slow decay of syn-MVKO is related to its resonance-stabilized electronic structure[32,36], which would be disrupted at the transition state of the unimolecular reaction[33,43]. Another interesting aspect of this resonance stabilization is that the iodine-atom adduct of MVKO is relatively less stable compared to the cases of alkyl CIs[36].

MACRO also has a resonance-stabilized electronic structure and two non-interconverting families of conformers (Fig. 1). It has also been predicted that syn-$trans$-MACRO (following the nomenclature of Vansco et al.)[34] would interconvert quickly ($>10^6 s^{-1}$) to syn-cis-MACRO, which would undergo fast unimolecular decay ($k_{uni} = 2500 s^{-1}$) to form dioxole, while $anti$ conformers are expected to have slow unimolecular decay (ca. $10 s^{-1}$)[32]. These theoretically predicted values are from Vereecken et al.[32] who utilized the structure–activity relationships which considered the best available theoretical and experimental results at that time. However, similar to other $anti$ types of CIs (CH_2OO and $anti$-CH_3CHOO)[17,18], the reaction of $anti$-MACRO with water vapor was predicted to be fast ($k_{water-eff} = 7.2 \times 10^{-15} cm^3 s^{-1}$ by Anglada et al.[44] or $6.3 \times 10^{-16} cm^3 s^{-1}$ by Vereecken et al.[32] at relative humidity (RH) = 70% and 298 K, considering both water monomer and dimer reactions). If so, the fast reaction with water vapor (ca. $10^3 s^{-1}$) would result in a very low steady-state concentration of $anti$-MACRO, diminishing its atmospheric impact. Nonetheless, as will be shown later, this picture is incorrect.

Very recently, Vansco et al. have reported the electronic spectroscopy and photochemistry of MACRO; as the authors have mentioned, "This UV–visible detection scheme will enable study of its unimolecular and bimolecular reactions under thermal conditions of relevance to the atmosphere."[34] Following their method, here we prepared MACRO starting from the photolysis of E-1,3-diiodo-2-methylprop-1-ene precursor (Fig. 1). The time-resolved UV–visible spectrum of MACRO was recorded by using a continuous broadband light source and a grating spectrometer equipped with an ultrafast CMOS camera. Analyzing the time series of the spectra allowed us to retrieve the spectrum of MACRO and its time-dependent concentration.

To our surprise, the reaction of MACRO with water vapor was found to be much slower than previous predictions[32,44] by one or two orders of magnitude, implying much longer atmospheric lifetime (ca. 18 ms vs. 3 or 0.3 ms[32,44]) and higher steady-state concentrations for atmospheric MACRO. On the other hand, the resonance-stabilized MACRO still reacts extremely fast with SO_2. Based on the results of a recent global chemistry and transportation model of MVKO[35], our data suggest that the impact of
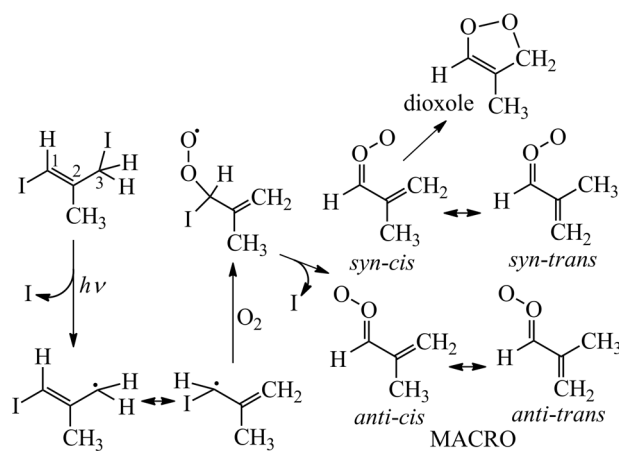
Fig. 1 Synthesis and conformers of methacrolein oxide (MACRO). We follow the method and nomenclature of Vansco et al.[34].
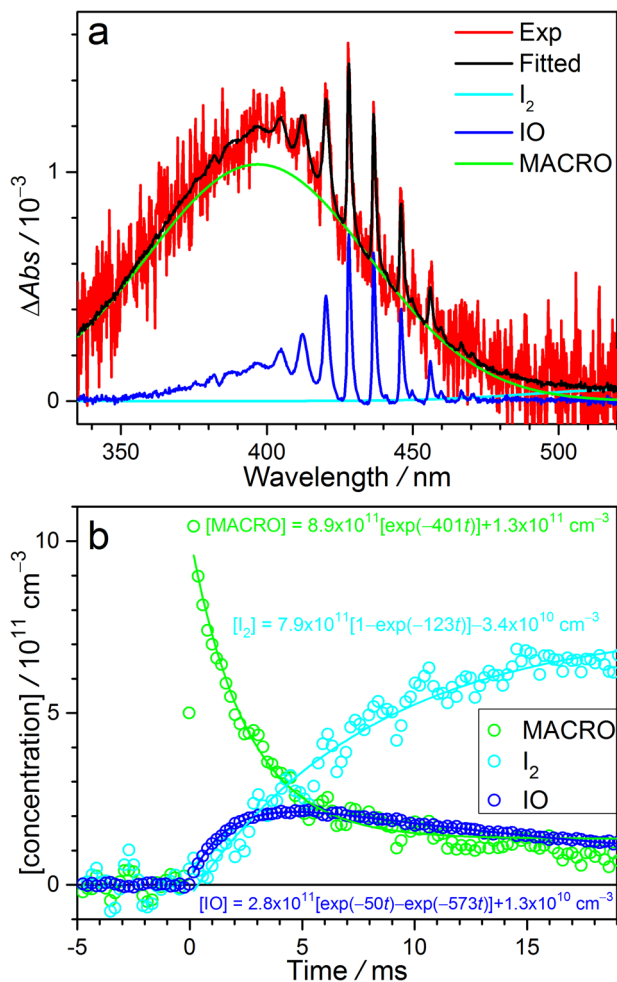
Fig. 2 Absorption spectra and their time evolutions. a The difference absorption spectrum recorded in the 1,3-diiodo-2-methylprop-1-ene/O_2 photolysis system at 298 K and 500 Torr at 0.4 ms photolysis-probe delay time (red line, the data is from Exp #13, see Supplementary Table 2). The absorption contributions of MACRO (green), IO (blue), and I_2 (cyan; black is the sum of MACRO, IO, and I_2) are also shown. **b** Concentrations of MACRO, IO, and I_2 obtained by fitting the spectra of Exp #13 at $[H_2O] = 0$ at each photolysis-probe delay time. [MACRO] is derived by using the reported peak cross section $= 3 \times 10^{-18}$ cm^2 by Vansco et al.[34], [IO] and [I_2] are estimated with literature cross sections[45,46] (see Supplementary Fig. 4).

MACRO on the oxidation of atmospheric SO_2 would also be substantial.

Results and discussion
Analysis of the observed UV spectrum. Figure 2a shows the time-resolved difference absorption spectra recorded in the photolysis reactor. Here 'difference' means the change after the photolysis laser pulse. We can see three spectral features in the spectrum: (i) a very broad and structureless absorption band peaking at ca. 397 nm; (ii) absorption of IO which has distinctive sharp peaks between 400 and 460 nm[45]; (iii) broad absorption band of I_2 extending to 520 nm[46]. The presence of IO and I_2 is similar to previous investigations of CH_2OO[47–49], CH_3CHOO[23,50], $(CH_3)_2COO$[51], and MVKO[35,36].

UV absorption spectrum of MACRO. Under the same experimental conditions, SO_2 was added to scavenge CIs (see Supplementary Fig. 1). We found that the spectral feature (i) disappears, indicating its spectral carrier is a Criegee intermediate. We
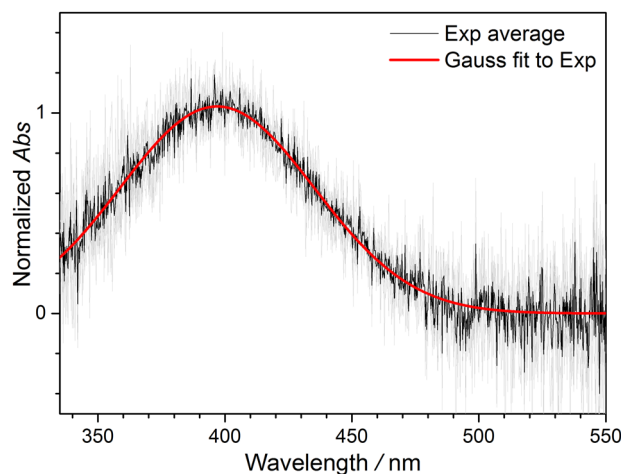
Fig. 3 Height-normalized spectra of MACRO. The spectra of MACRO are obtained from the difference spectra between the spectra without SO_2 and the spectra with $[SO_2] \cong 10^{14}$ cm^{-3} at 0.18 ms delay time. Four spectra obtained from Exp #1−4 are plotted as gray lines, and their average is plotted as a black line. The red curve shows the Gaussian fit to the average spectrum with peak position 397 nm and full width at half-maximum (FWHM) 77 nm.

further subtracted the time-resolved spectra recorded at $[SO_2] = 1 \times 10^{14}$ cm^{-3} from those without adding SO_2 at each photolysis-probe delay time. This operation removed most of the absorption signals of IO and I_2 (and also other minor byproducts), and the resulted spectra would be mainly from the Criegee intermediate. Considering that we were using the same precursor and preparation method of Vansco et al.[34], we assigned this CI to MACRO.

The spectrum of MACRO can be well fitted with a Gaussian function (Fig. 3). This spectrum is similar to that of Vansco et al. who reported a broad spectrum of MACRO peaked at 380 nm with weak oscillatory structure at long wavelengths ascribed to vibrational resonances[34]. However, we do not observe such oscillatory structure; the differences are presumably due to different temperatures of the MACRO samples (thus, the conformer populations may be different), as Vansco et al. recorded their spectrum under a jet cool condition[34].

We may decompose the observed spectra into the contributions of MACRO, IO, and I_2 (Fig. 2a and Supplementary Fig. 4) with a least-squares fit. The resulted signal intensities (converted to concentrations) of MACRO, IO, and I_2 are plotted in Fig. 2b as a function of the delay time. The intensities of IO and I_2 grow with time, indicating they are secondary products. While the kinetics of IO and I_2 formation may be interesting, we like to focus on MACRO in this work. We can see that the lifetime of MACRO in this particular experiment is ca. 3 ms, much longer than the predicted value for *syn*-MACRO (<0.4 ms, based on its $k_{uni} = 2500$ s^{-1}[32]; and other chemical processes would further shorten the lifetime). Therefore, we conclude that the observed spectral carrier should be *anti*-MACRO, similar to the case of MVKO[35]. Note that the long lifetime conformer of MVKO is *syn*-MVKO (following the nomenclature of Barbar et al.)[33] which has a structure similar to *anti*-MACRO. For simplicity, we will use MACRO to represent *anti*-MACRO in the following analysis.

Kinetics of MACRO reaction with SO_2. The above analysis has been repeated for experiments adding various $[SO_2]$. The resulted MACRO signal intensities at each photolysis-probe delay time are plotted in Fig. 4a. The decay of MACRO signal can be fitted with a single exponential function to yield a pseudo-first-order rate

3
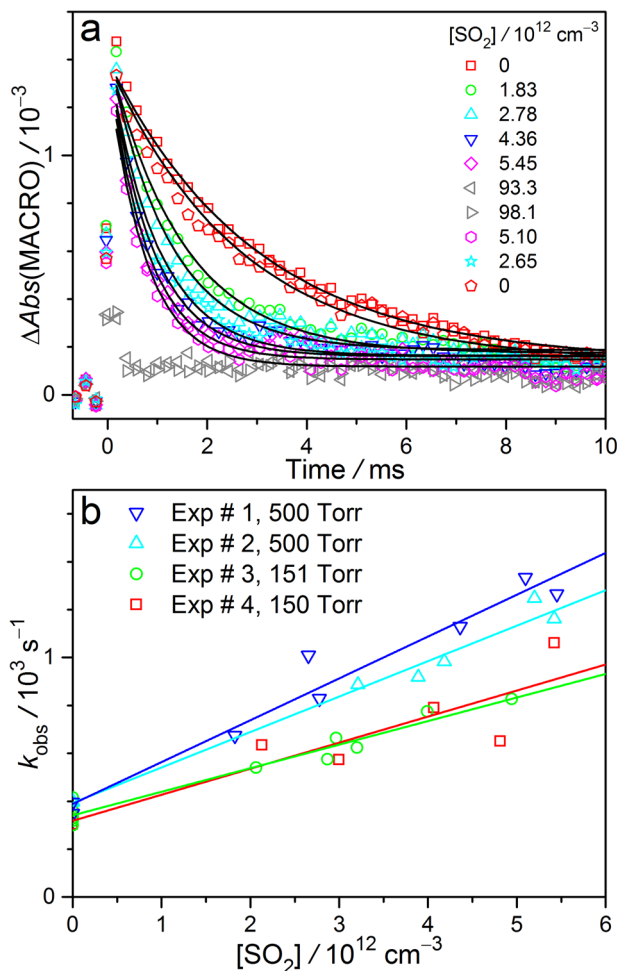
Fig. 4 Kinetic plots of MACRO + SO$_2$. a Time profiles of the absorbance changes of MACRO obtained by fitting the spectra at each delay time under various [SO$_2$] at 298 K and 500 Torr. The data are from Exp #1. The black curves show the fitting results of single exponential decay. **b** Pseudo-first-order plot of the reaction rate coefficients of MACRO with SO$_2$ at 298 K.

coefficient, k_{obs}, at each [SO$_2$].

$$\Delta Abs(MACRO) = \sigma L[MACRO](t) = \sigma L[MACRO]_0 \exp(-k_{obs}t)$$

where σ is the absorption cross section of MACRO[34] and L is the optical path length (when reporting ΔAbs(MACRO), we use its peak value at 397 nm). Figure 4b shows that k_{obs} increases linearly with [SO$_2$].

$$k_{obs} = k_0 + k_{SO2}[SO_2]$$

The slope would correspond to the rate coefficient k_{SO2} of the bimolecular reaction of MACRO with SO$_2$, while the intercept k_0 would account for other decay processes of MACRO that are independent on [SO$_2$], like reactions with radical byproducts (including MACRO self-reaction), unimolecular decay, etc.

Because that MACRO can be fully scavenged within 0.3 ms under a high [SO$_2$] ($\geq 9.3 \times 10^{13}$ cm^{-3}), we may further improve the analysis by subtracting the high [SO$_2$] spectrum (the average spectrum at the two highest [SO$_2$]) from other low [SO$_2$] spectra to remove most of the byproduct contributions while some minor amounts of IO and I$_2$ may still remain (SO$_2$ scavenge method). The resulted spectra were then decomposed into the contributions of MACRO and IO and I$_2$. The time profiles of MACRO are plotted in Supplementary Fig. 2. When using this SO$_2$ scavenge method, we
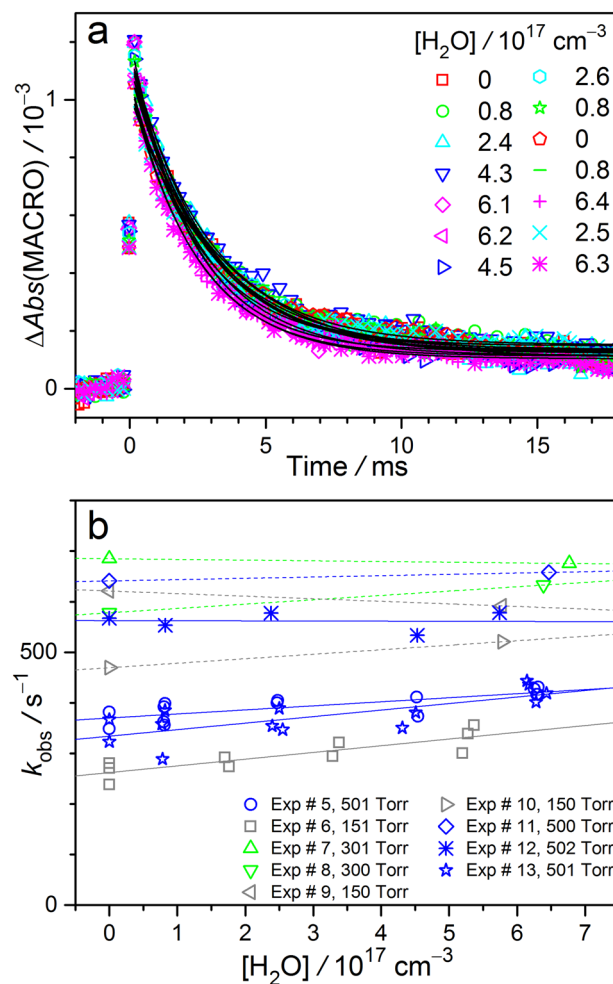
Fig. 5 Kinetic plots of MACRO + H$_2$O. a Time profiles of the MACRO absorption signal obtained by fitting the spectra at each delay time under various [H$_2$O] at 298 K and 501 Torr. The data are from Exp #13 (Supplementary Table 2). The black curves show the fitting results of a single exponential decay function. **b** The pseudo-first-order plot of the reaction rate coefficients of MACRO with H$_2$O at 298 K.

did not include the data point at the first delay time (0.18 ms) due to incomplete scavenging.

The kinetic results of MACRO + SO$_2$ reaction are summarized in Supplementary Table 1. The data at 150 and 500 Torr do not show significant difference after considering the experimental uncertainties. For these four sets of experimental data, we report the rate coefficient to be $(1.5 \pm 0.4) \times 10^{-10}$ cm^3 s^{-1} at 298 K and 150–500 Torr ($\pm 1\sigma$, σ is the standard deviation of the data). The rate coefficients of SO$_2$ reactions with other CIs (CH$_2$OO[5,52], *anti*- and *syn*-CH$_3$CHOO[21,23], (CH$_3$)$_2$COO[30,51], MVKO[35,36]) are in the range of $(0.4–2.2) \times 10^{-10}$ cm^3 s^{-1}[17,18]. It appears that the resonance-stabilization of *anti*-MACRO does not reduce its reactivity towards SO$_2$.

Kinetics of MACRO reaction with H$_2$O. The same method has been applied to investigate the kinetics of MACRO reaction with water vapor. To our surprise, the effect of water in the decay of MACRO is rather weak as shown in Fig. 5, indicating slow reaction. From the plots of k_{obs} as a function of [H$_2$O] (Fig. 5b), we can see that the slopes are quite insignificant; some of them are even negative, indicating that these rate measurements are close to our measurement limit (see Supplementary Table 2). Note that the highest [H$_2$O] used is ca. 6×10^{17} cm^{-3} (ca. 18

Table 1 Summary of theoretically estimated unimolecular rate coefficient k_{uni} and bimolecular rate coefficients of the reactions with water monomer and dimer (k_{H2O} and $k_{(H2O)2}$) at 298 K for selected CIs.

Relative humidity				70%		35%		
$[H_2O]/10^{17}$ cm^{-3}				5.4		2.7		
$[(H_2O)_2]/10^{14}$ cm^{-3}				6.7		1.7		
CI	k_{uni} (s^{-1})	k_{H2O} (cm^3 s^{-1})	$k_{(H2O)2}$ (cm^3 s^{-1})	$k_{water-eff}$ [a] (cm^3 s^{-1})	k_{atm} [b] (s^{-1})	$k_{water-eff}$ [a] (cm^3 s^{-1})	k_{atm} [b] (s^{-1})	Ref.
syn-MVKO	33	3.4×10^{-19}	9.2×10^{-16}	1.5×10^{-18}	34	9.1×10^{-19}	33	35,44
	50	8.1×10^{-20}	3.1×10^{-16}	4.6×10^{-19}	50	2.7×10^{-19}	50	32
	[70 ± 15]	–	–	—	70	—	70	43
anti-MACRO	–	3.0×10^{-15}	3.4×10^{-12}	7.2×10^{-15}	3900	5.1×10^{-15}	1400	44
	10	1.9×10^{-16}	3.6×10^{-13}	6.3×10^{-16}	350	4.1×10^{-16}	120	32
	< 25	4.9×10^{-17}	1.6×10^{-14}	6.9×10^{-17}	< 62	5.9×10^{-17}	< 41	Theory[c]
	7[d]	–	–	$[(9 \pm 5) \times 10^{-17}]$	56	$[(9 \pm 5) \times 10^{-17}]$	31	This work
syn-MACRO	—	2.3×10^{-19}	2.4×10^{-15}	1.3×10^{-17}	–	1.7×10^{-18}	—	44
	2500	1.5×10^{-19}	5.6×10^{-16}	8.4×10^{-19}	2500	5.0×10^{-19}	2500	32
	2600	1.4×10^{-20}	4.1×10^{-17}	6.4×10^{-20}	2600	3.9×10^{-20}	2600	Theory[c]

Available experimental results are shown in square brackets.
[a] $k_{water-eff} = (k_{H2O}[H_2O] + k_{(H2O)2}[(H_2O)_2])/[H_2O]$ at 298 K, in which $[(H_2O)_2]$ is estimated with $K_{eq} = P_{dimer}/P_{monomer}^2 = 0.0556$ bar^{-1} reported by Anglada et al.[53]
[b] $k_{atm} = k_{uni} + k_{water-eff}[H_2O]$.
[c] This work, based on QCISD(T)/CBS//B3LYP/6-311+G(2d,2p) (CBS = complete basis set extrapolated).
[d] Our best estimated theoretical value (see text).

Torr), which has replaced a larger portion (18/150 = 12%) of the bath gas if the total pressure is only 150 Torr (N_2 balance). Thus, we think it may require some cautions to view the data of 150 Torr, because the reaction environment (type of bath gas) changes at various $[H_2O]$. Nonetheless, no trend can be found for pressures from 150 to 500 Torr. Finally, we chose the weighted average from six experimental sets (300 and 500 Torr and 298 K, Supplementary Table 2), to report the effective rate coefficient for the reaction of MACRO with water vapor, $k_{water-eff} = (9 \pm 5) \times 10^{-17}$ cm^3 s^{-1} ($\pm 1\sigma$). As mentioned above, we are not confident enough to determine the lower limit of $k_{water-eff}$.

MACRO isomers. As pointed out by Vereecken et al., the *cis–trans* interconversion (Supplementary Fig. 6) ($>10^6$ s^{-1}) is orders-of-magnitude faster than other chemical processes, such that the *cis* and *trans* conformers will be in near-equilibrium and should be considered as a single pool of species[32]. Following this idea, we summarize the rate coefficients of the unimolecular processes and reactions with water vapor (monomer and dimer[53]) in Table 1 for relevant CIs[32,35,43,44].

As shown in Table 1, the predicted unimolecular decay rates are very different for *syn-* and *anti-*MACRO. *Syn-*MACRO would have a rather short lifetime of ca. $1/2500 = 4 \times 10^{-4}$ s[32], which means its steady-state concentration would be very low. The experimental lifetime of MACRO is found to depend on the signal intensity—the higher the signal is, the shorter the lifetime. This is due to the fact that the inevitable reactions of MACRO with radical byproducts, including I atoms, IO radicals, MACRO itself and the products from the fast decomposition of *syn-*MACRO (similar to the case of *anti-*MVKO)[42] would shorten its lifetime. Supplementary Fig. 3 shows the plot of k_{obs} against $[MACRO]_0$. The linear relationship supports the above mechanism. Extrapolating k_{obs} to zero $[MACRO]_0$ would effectively remove the bimolecular contributions and give an estimate for the unimolecular lifetime of MACRO. The preliminary data of Supplementary Fig. 3 are consistent with $k_{uni} \cong k_{obs}([MACRO]_0 = 0) < 50$ s^{-1}, which gives a lifetime > 20 ms. This long-lived MACRO cannot be *syn-*MACRO. Thus, the observed signal should belong to *anti-*MACRO.

Compare of $k_{water-eff}$ with previous theory. The value of $k_{water-eff}$ of *anti-*MACRO (Table 1) is smaller than those of CH_2OO and

anti-CH_3CHOO[17,18] by orders of magnitude, suggesting that the extended conjugation of *anti-*MACRO correlates with the lower reactivity towards water vapor (monomer and dimer), since the alkyl-substituted CIs lack the resonance-stabilized electronic structure of the extended conjugation.

Anglada et al. have predicted the rate coefficients for *anti-*MACRO reactions with water monomer and dimer, giving $k_{water-eff} = 7.2 \times 10^{-15}$ cm^3 s^{-1} at RH = 70% and 298 K (Table 1)[44]. To our surprise, this value is ca. 80 times larger than our experimental value. However, Vereecken et al. have pointed out that the level of theory used by Anglada et al.[44] tends to underestimate the barriers for the CI reactions with water monomer and dimer[32]. Using 'structure–activity relationship', Vereecken et al. scaled the barrier heights of a number of CI reactions by considering the best known theoretical and experimental data (mainly for CH_2OO and *anti-*/*syn-*CH_3CHOO) at that time[32]. The resulted rate coefficients of MACRO are also shown in Table 1. We can see this 'scaling' does reduce the gap (from 80 times to 7 times) between the theoretical predictions and our experimental data. Since the reference data in the work of Vereecken et al.[32] do not contain trustable data for reactions of CIs having a conjugated C=C group (i.e., there is no good anchor point for the scaling), this difference may be reasonable. Also note that Vereecken et al.[32] have estimated an uncertainty of one order of magnitude for their rate coefficients at 298 K.

With details given in Supplementary Note 3, we found that it is important to calculate the reaction barrier heights at a high level of quantum chemistry theory like QCISD(T)/CBS//B3LYP/6-311+G(2d,2p) (CBS = complete basis set extrapolation)[54–60]. For example, the QCISD(T)/CBS barriers are ca. 1.4 or 2.0 kcal mol^{-1} higher than those calculated at QCISD(T)/aug-cc-pVTZ (AVTZ) for various reactions between (CH_2=CH)CHOO conformers with H_2O monomer or dimer (Supplementary Fig. 7 and Supplementary Table 4), indicating that only using the AVTZ barrier heights would overestimate the reaction rates significantly.

After properly scaling the effect of the basis sets (CBS vs. AVTZ) by using the results of (CH_2=CH)CHOO, which has a structure similar to MACRO, as an anchor point, (Supplementary Fig. 7)[54] our calculation (Table 1) also predicts slower rates compared to previous ones.

Compare of $k_{\text{water-eff}}$ with ozonolysis experiment. Newland et al. have analyzed the effect of water vapor in the system of isoprene ozonolysis; in their two-CI model, the isoprene-derived non-CH_2OO CI (sum of MVKO and MACRO) has an effective reaction rate coefficient with water vapor of $(1.1 \pm 0.27) \times 10^{-15} \text{ cm}^3 \text{ s}^{-1}$[61]. While all conformers of MVKO are expected to react with water vapor much slower ($k_{\text{water-eff}} \leq 10^{-17} \text{ cm}^3 \text{ s}^{-1}$)[44], the value of Newland et al. is much larger than our $k_{\text{water-eff}}$ for MACRO. At the time (2015) when the work of Newland et al. was published, the knowledge of the reaction kinetics of MVKO and MACRO was not available at all. As multiple CIs are produced in the isoprene ozonolysis system, the kinetics is rather complicated, especially when these CIs have very different reactivities towards water vapor. For example, CH_2OO, which has the predominant yield in the isoprene ozonolysis system[2,3], would be quickly consumed by its reaction with water vapor, but MVKO and MACRO would not. See Supplementary Note 2 for an alternative analysis to fit the data of Newland et al.[61]. In fact, Newland et al. have mentioned that the competing effects of the different kinetics of two distinct forms (*syn* and *anti* conformers) in the system may effectively lead to one masking the other under the experimental conditions applied[61].

Best estimation of k_{uni}. It is very difficult to experimentally measure the very slow rate of the *anti*-MACRO unimolecular reaction. While our preliminary experimental data (Supplementary Fig. 3) suggest that the unimolecular reaction is slow, we cannot nail down the value of k_{uni} by the experimental results. On the theoretical side, the unimolecular reaction of *anti*-MACRO proceeds through the OO bending channel forming dioxirane[32,34,39], similar to that of CH_2OO[41,62]. By comparing with the results of high-accuracy extrapolation protocols like HEAT-345(Q)[62] or high-level multireference methods like MRCI+Q (Davidson correction)/CBS[41], Yin and Takahashi have found that the QCISD(T)/CBS method slightly underestimates the barrier height of this channel (by ca. 0.4 or 1.2 kcal mol^{-1}, respectively) for CH_2OO[41]. Our analysis in Supplementary Note 3 shows that for the MACRO unimolecular reaction, the electronic energy obtained by QCISD(T)/CBS would consistently underestimate the barrier height and other factors in the rate calculation, like hindered-rotor partition function calculation and tunneling correction, have very minor effects compared to that of the electronic energy. Therefore, our theoretical value (25 s^{-1}) of k_{uni} of *anti*-MACRO would only represent an upper limit.

Assuming such underestimation in the barrier heights (0.4 or 1.2 kcal mol^{-1}) is similar for the unimolecular reactions of MACRO and CH_2OO, we may have an overestimation of a factor of 2 or 7 for the reaction rate coefficient at 298 K. Thus, we think the best estimated k_{uni} at 298 K would be ca. $25/(2 \times 7)^{0.5} = 7 \text{ s}^{-1}$ (the uncertainty may be up to a factor of 3), which is (almost) coincident with the theoretical value of 10 s^{-1} by Vereecken et al. (claimed uncertainty is ca. a factor of 5 for non-H-migration reactions)[32]. Although the uncertainty is still not very small, "for many assessments, however, it is sufficient to determine whether the reaction is significantly faster or slower than competing reactions", mentioned by Vereecken et al.[32].

Atmospheric lifetime. Because the unimolecular decay and reaction with water vapor are the predominant processes that determine the atmospheric lifetime of a CI[17,18,32], we may estimate the effective decay rate coefficient k_{atm} for atmospheric *anti*-MACRO.

$$k_{\text{atm}} = k_{\text{uni}} + k_{\text{water-eff}}[H_2O]$$

Taking the best estimated k_{uni} (7 s^{-1}) and our experimental data of $k_{\text{water-eff}}$ (Table 1), we have $k_{\text{atm}} = 56 \text{ s}^{-1}$ (or $<74 \text{ s}^{-1}$, if taking our theoretical upper limit of 25 s^{-1} for k_{uni}) for *anti*-

MACRO at RH = 70% and 298 K. Note that the water reaction may still predominate in the decay processes of atmospheric *anti*-MACRO under humid conditions that are typical for tropical forests where the isoprene emission is large. And this atmospheric lifetime (ca. 18 ms, best estimate) is much longer than previously thought (0.3 or 3 ms, see Table 1), indicating that the atmospheric concentration of *anti*-MACRO would be much higher than previously expected. If using the upper limits of k_{uni} (25 s^{-1}) and $k_{\text{water-eff}}[H_2O]$ ($49 + 54 = 103 \text{ s}^{-1}$, 2σ upper bound, at RH = 70% and 298 K), we then have $k_{\text{atm}} < 128 \text{ s}^{-1}$, which would correspond to a lifetime longer than 7.8 ms.

Impact of *anti*-MACRO on the oxidation of atmospheric SO_2. This would depend on three factors: (i) the yield of *anti*-MACRO in the ozonolysis of atmospheric alkenes (mainly isoprene), (ii) the atmospheric lifetime of *anti*-MACRO, and (iii) the rate coefficient of *anti*-MACRO reaction with SO_2. Each factor is discussed below.

First, based on the recent analysis of Nguyen et al., *anti*-MACRO has a yield of 15% among all stabilized CIs in isoprene ozonolysis, which is very similar to that of *syn*-MVKO (14%)[2,17]. In addition, an earlier study of Zhang and Zhang has shown that the activation energies of O_3 cycloaddition to the two double bonds of isoprene are comparable and the barrier heights from the primary ozonides to *syn*-MVKO and *anti*-MACRO are also similar, implying that the *syn*-MVKO and *anti*-MACRO pathways are both accessible[4].

Second, given that *syn*-MACRO and *anti*-MVKO have much shorter lifetimes ($\tau < 1$ ms), the oxidation of atmospheric SO_2 by the C4 CIs from isoprene ozonolysis would be mainly by *anti*-MACRO and *syn*-MVKO ($\tau > 10$ ms)[32,35]. The order of magnitude of k_{atm} of *anti*-MACRO (56 s^{-1}) is comparable to that of *syn*-MVKO ($k_{\text{atm}} \cong k_{\text{uni}} = 33 \text{ s}^{-1}$ or 70 s^{-1}[33,43]; $k_{\text{water-eff}} \sim 10^{-18} \text{ cm}^3 \text{ s}^{-1}$)[32,35]. Combined with their similar yields in the isoprene ozonolysis, this suggests that *anti*-MACRO and *syn*-MVKO would have similar steady-state concentrations ($[\text{anti-MACRO}]_{ss} \approx [\text{syn-MVKO}]_{ss}$) in the troposphere.

Finally, the rate coefficient of SO_2 reaction with *anti*-MACRO, $(1.5 \pm 0.4) \times 10^{-10} \text{ cm}^3 \text{ s}^{-1}$, is larger than that with *syn*-MVKO, $(4.0 - 4.2) \times 10^{-11} \text{ cm}^3 \text{ s}^{-1}$[35,36], by a factor of ca. 4. Overall, the oxidation rate of SO_2 by *anti*-MACRO would be larger than that by *syn*-MVKO by a factor of $([\text{anti-MACRO}]_{ss}/[\text{syn-MVKO}]_{ss})$ ($k_{\text{SO2\_anti-MACRO}}/k_{\text{SO2\_syn-MVKO}}$). This factor would be larger than unity, if we assume that these two CIs are mainly from isoprene ozonolysis with similar yields.

Although CH_2OO has the highest yield (ca. 58%) among the stabilized CIs produced in the ozonolysis of isoprene[2,17], its fast reaction with water vapor results in a rather short atmospheric lifetime (<1 ms)[17–20], too short for CH_2OO to reach any substantial concentration to oxidize atmospheric SO_2. Recently Caravan et al., who utilized the up-to-date data of MVKO kinetics, show that *syn*-MVKO has the largest modeled steady-state concentration among all stabilized CIs globally (33% by molecules, 49% by weight)[35]. The above analysis shows that *anti*-MACRO would have similar concentrations as those of *syn*-MVKO and an even larger impact on the SO_2 oxidation.

Conclusion
Following the method of Vansco et al.[34], MACRO has been synthesized and its UV–visible spectroscopy and reaction kinetics have been investigated. Similar to MVKO, MACRO has two non-interconverting isomers, *syn* and *anti* forms. *Syn*-MACRO would undergo fast 1,5-ring closure with a predicted thermal lifetime of <0.4 ms. In our experiments, a much longer lifetime ($\tau > 4$ ms) has been observed, indicating that the spectral carrier is *anti*-

MACRO. The rate coefficient of *anti*-MACRO reaction with SO_2 has been determined to be $(1.5 \pm 0.4) \times 10^{-10}$ cm^3 s^{-1} at 298 K, which is substantially larger than that of the *syn*-MVKO + SO_2 reaction. However, the reaction of *anti*-MACRO with H_2O was found to be quite slow with an effective rate coefficient of $(9 \pm 5) \times 10^{-17}$ cm^3 s^{-1} at 298 K, which is smaller than previous theoretical values by 1 or 2 orders of magnitude. Theoretical calculations that properly treat the effect of the conjugated C=C substitution may reproduce the experimental trend.

A recent global chemistry and transport modeling based on the most up-to-date knowledge of MVKO chemistry has shown that *syn*-MVKO is important in the tropospheric processes of SO_2 oxidation and formic acid removal[35]. Our results indicate that *anti*-MACRO has an atmospheric lifetime similar to that of *syn*-MVKO, resulting in a similarly substantial steady-state concentration. Combined with the larger rate coefficient of its reaction with SO_2, the impact of *anti*-MACRO on the oxidation of atmospheric SO_2 would be larger than (at least comparable to) that of *syn*-MVKO.

As mentioned above, to serve as an efficient oxidant of SO_2, it is required to have a long-enough lifetime under atmospherically relevant conditions. As shown above and in the literature[35], a resonance-stabilized electronic structure plays an interesting role for CIs. It reduces the reactivity for unimolecular decay and reactions with water vapor, but not for the reactions with SO_2. Thus, having a resonance-stabilized electronic structure may be a new direction for searching for a long-lived CI that is able to oxidize atmospheric SO_2.

Methods
MACRO preparation. The experimental setup has been published[19,36]. We prepared MACRO following Vansco et al.: ICHC(CH$_3$)CH$_2$I (1,3-diiodo-2-methyl-prop-1-ene, Accela, 97.8% by gas chromatography) + $h\nu$ (248 nm) → CH$_2$=C(CH$_3$)CHI + I, CH$_2$=C(CH$_3$)CHI + O$_2$ → CH$_2$=C(CH$_3$)CHOO + I (Fig. 1)[34]. The precursor concentrations were determined by its UV absorption spectra; the absolute cross sections (Supplementary Fig. 4) have been determined by measuring the weight loss of the precursor sample and the volume flow rate of the dilution gas[63,64] (see Supplementary Note 1).

CMOS camera spectrometer. A grating spectrometer (Andor SR303i) and fast CMOS camera (Andor, Marana-4BU11) were used to obtain the time-resolved absorption spectra of the reaction system. A series of spectra (exposure time 0.21 ms (or 0.43 ms) each) were recorded for every photolysis event. The spectrum taken before the photolysis laser pulse was used as the reference spectrum; therefore, the change of absorbance caused by the photolysis laser pulse was recorded transiently. Accumulation of 256, 512 (0.43 ms exposure time), or 1280, 2560 (0.21 ms exposure time) laser pulses was performed to improve the signal-to-noise ratio.

A background spectrum (without adding the MACRO precursor 1,3-diiodo-2-methylprop-1-ene) was recorded under the same experimental condition. This background was due to the interaction between the photolysis laser beam and the used optics (mainly the long-pass filters that reflected the photolysis laser beam and transmitted the probe beam). All the reported spectra are background corrected.

Theoretical calculations. We optimized the reactant and transition state geometries on the singlet ground electronic state using B3LYP/6-311+G(2*d*,2*p*)[54,58,59]. See Supplementary Data 1 for the optimized XYZ geometries. The electronic energies were corrected at QCISD(T)/CBS level[54–60], except for the transition states of MACRO + 2H$_2$O, of which the energies were estimated with a correction method detailed in Supplementary Note 3 (Supplementary Figs. 7–9, Supplementary Tables 4–6). The rate coefficients were calculated using the conventional transition state theory method using rigid rotor harmonic oscillator approximations including tunneling correction.

Data availability
The data supporting the findings of this study are available within the article, its Supplementary Information, and Supplementary Data 1 (XYZ geometries), and from the corresponding author upon reasonable request.

References
1. Sindelarova, K. et al. Global data set of biogenic VOC emissions calculated by the MEGAN model over the last 30 years. *Atmos. Chem. Phys.* **14**, 9317–9341 (2014).
2. Nguyen, T. B. et al. Atmospheric fates of Criegee intermediates in the ozonolysis of isoprene. *Phys. Chem. Chem. Phys.* **18**, 10241–10254 (2016).
3. Aschmann, S. M. & Atkinson, R. Formation yields of methyl vinyl ketone and methacrolein from the gas-phase reaction of O$_3$ with isoprene. *Environ. Sci. Technol.* **28**, 1539–1542 (1994).
4. Zhang, D. & Zhang, R. Mechanism of OH formation from ozonolysis of isoprene: a quantum-chemical study. *J. Am. Chem. Soc.* **124**, 2692–2703 (2002).
5. Welz, O. et al. A direct kinetic measurements of Criegee intermediate (CH$_2$OO) formed by reaction of CH$_2$I with O$_2$. *Science* **335**, 204–207 (2012).
6. Srivastava, R. K., Miller, C. A., Erickson, C. & Jambhekar, R. Emissions of sulfur trioxide from coal-fired power plants. *J. Air Waste Manag. Assoc.* **54**, 750–762 (2004).
7. Liu, T. et al. Formation of secondary aerosols from gasoline vehicle exhaust when mixing with SO$_2$. *Atmos. Chem. Phys.* **16**, 675–689 (2016).
8. Sipilä, M. et al. The role of sulfuric acid in atmospheric nucleation. *Science* **327**, 1243 (2010).
9. Mauldin Iii, R. L. et al. A new atmospherically relevant oxidant of sulphur dioxide. *Nature* **488**, 193–196 (2012).
10. Boy, M. et al. Oxidation of SO$_2$ by stabilized Criegee intermediate (sCI) radicals as a crucial source for atmospheric sulfuric acid concentrations. *Atmos. Chem. Phys.* **13**, 3865–3879 (2013).
11. Stangl, C. M. et al. Sulfur dioxide modifies aerosol particle formation and growth by ozonolysis of monoterpenes and isoprene. *J. Geophys. Res. Atmos.* **124**, 4800–4811 (2019).
12. Díaz-de-Mera, Y. et al. Formation of secondary aerosols from the ozonolysis of styrene: effect of SO$_2$ and H$_2$O. *Atmos. Environ.* **171**, 25–31 (2017).
13. Ye, J., Abbatt, J. P. D. & Chan, A. W. H. Novel pathway of SO$_2$ oxidation in the atmosphere: reactions with monoterpene ozonolysis intermediates and secondary organic aerosol. *Atmos. Chem. Phys.* **18**, 5549–5565 (2018).
14. Liu, L. et al. Effects of stabilized Criegee intermediates (sCIs) on sulfate formation: a sensitivity analysis during summertime in Beijing–Tianjin–Hebei (BTH), China. *Atmos. Chem. Phys.* **19**, 13341–13354 (2019).
15. Green, J. R. et al. Rates of wintertime atmospheric SO$_2$ oxidation based on aircraft observations during clear-sky conditions over the eastern United States. *J. Geophys. Res. Atmos.* **124**, 6630–6649 (2019).
16. Novelli, A. et al. Estimating the atmospheric concentration of Criegee intermediates and their possible interference in a FAGE-LIF instrument. *Atmos. Chem. Phys.* **17**, 7807–7826 (2017).
17. Cox, R. A. et al. Evaluated kinetic and photochemical data for atmospheric chemistry: Volume VII—Criegee intermediates. *Atmos. Chem. Phys.* **20**, 13497–13519 (2020).
18. Lin, J. J.-M. & Chao, W. Structure-dependent reactivity of Criegee intermediates studied with spectroscopic methods. *Chem. Soc. Rev.* **46**, 7483–7497 (2017).
19. Chao, W., Hsieh, J.-T., Chang, C.-H. & Lin, J. J.-M. Direct kinetic measurement of the reaction of the simplest Criegee intermediate with water vapor. *Science* **347**, 751 (2015).
20. Smith, M. C. et al. Strong negative temperature dependence of the simplest Criegee intermediate CH$_2$OO reaction with water dimer. *J. Phys. Chem. Lett.* **6**, 2708–2713 (2015).
21. Taatjes, C. A. et al. Direct measurements of conformer-dependent reactivity of the Criegee intermediate CH$_3$CHOO. *Science* **340**, 177–180 (2013).
22. Lin, L.-C., Chao, W., Chang, C.-H., Takahashi, K. & Lin, J. J.-M. Temperature dependence of the reaction of *anti*-CH$_3$CHOO with water vapor. *Phys. Chem. Chem. Phys.* **18**, 28189–28197 (2016).
23. Sheps, L., Scully, A. M. & Au, K. UV absorption probing of the conformer-dependent reactivity of a Criegee intermediate CH$_3$CHOO. *Phys. Chem. Chem. Phys.* **16**, 26701–26706 (2014).
24. Li, Y.-L., Kuo, M.-T. & Lin, J. J.-M. Unimolecular decomposition rates of a methyl-substituted Criegee intermediate *syn*-CH$_3$CHOO. *Rsc Adv.* **10**, 8518–8524 (2020).
25. Smith, M. C., Chao, W., Takahashi, K., Boering, K. A. & Lin, J. J.-M. Unimolecular decomposition rate of the Criegee intermediate (CH$_3$)$_2$COO measured directly with UV absorption spectroscopy. *J. Phys. Chem. A* **120**, 4789–4798 (2016).
26. Stephenson, T. A. & Lester, M. I. Unimolecular decay dynamics of Criegee intermediates: energy-resolved rates, thermal rates, and their atmospheric impact. *Int. Rev. Phys. Chem.* **39**, 1–33 (2020).
27. Fang, Y., Barber, V. P., Klippenstein, S. J., McCoy, A. B. & Lester, M. I. Tunneling effects in the unimolecular decay of (CH$_3$)$_2$COO Criegee intermediates to OH radical products. *J. Chem. Phys.* **146**, 134307 (2017).

28. Fang, Y. et al. Deep tunneling in the unimolecular decay of CH_3CHOO Criegee intermediates to OH radical products. *J. Chem. Phys.* **145**, 234308 (2016).

29. Fang, Y. et al. Communication: real time observation of unimolecular decay of Criegee intermediates to OH radical products. *J. Chem. Phys.* **144**, 061102 (2016).

30. Chhantyal-Pun, R. et al. Direct measurements of unimolecular and bimolecular reaction kinetics of the Criegee intermediate $(CH_3)_2COO$. *J. Phys. Chem. A* **121**, 4–15 (2017).

31. Liu, F., Beames, J. M., Petit, A. S., McCoy, A. B. & Lester, M. I. Infrared-driven unimolecular reaction of CH_3CHOO Criegee intermediates to OH radical products. *Science* **345**, 1596 (2014).

32. Vereecken, L., Novelli, A. & Taraborrelli, D. Unimolecular decay strongly limits the atmospheric impact of Criegee intermediates. *Phys. Chem. Chem. Phys.* **19**, 31599–31612 (2017).

33. Barber, V. P. et al. Four-carbon Criegee intermediate from isoprene ozonolysis: methyl vinyl ketone oxide synthesis, infrared spectrum, and OH production. *J. Am. Chem. Soc.* **140**, 10866–10880 (2018).

34. Vansco, M. F. et al. Synthesis, electronic spectroscopy, and photochemistry of methacrolein oxide: a four-carbon unsaturated Criegee intermediate from isoprene ozonolysis. *J. Am. Chem. Soc.* **141**, 15058–15069 (2019).

35. Caravan, R. L. et al. Direct kinetic measurements and theoretical predictions of an isoprene-derived Criegee intermediate. *Proc. Nat. Acad. Sci. USA* **117**, 9733–9740 (2020).

36. Lin, Y.-H., Li, Y.-L., Chao, W., Takahashi, K. & Lin, J. J.-M. The role of the iodine-atom adduct in the synthesis and kinetics of methyl vinyl ketone oxide —a resonance-stabilized Criegee intermediate. *Phys. Chem. Chem. Phys.* **22**, 13603–13612 (2020).

37. Vansco, M. F., Marchetti, B. & Lester, M. I. Electronic spectroscopy of methyl vinyl ketone oxide: a four-carbon unsaturated Criegee intermediate from isoprene ozonolysis. *J. Chem. Phys.* **149**, 244309 (2018).

38. Kuwata, K. T., Hermes, M. R., Carlson, M. J. & Zogg, C. K. Computational Studies on the isomerization and hydration reactions of acetaldehyde oxide and methyl vinyl carbonyl oxide. *J. Phys. Chem. A* **114**, 9192–9204 (2010).

39. Kuwata, K. T. & Valin, L. C. Quantum chemical and RRKM/master equation studies of isoprene ozonolysis: methacrolein and methacrolein oxide. *Chem. Phys. Lett.* **451**, 186–191 (2008).

40. Kuwata, K. T., Valin, L. C. & Converse, A. D. Quantum chemical and master equation studies of the methyl vinyl carbonyl oxides formed in isoprene ozonolysis. *J. Phys. Chem. A* **109**, 10710–10725 (2005).

41. Yin, C. & Takahashi, K. How does substitution affect the unimolecular reaction rates of Criegee intermediates? *Phys. Chem. Chem. Phys.* **19**, 12075–12084 (2017).

42. Vansco, M. F. et al. Experimental evidence of dioxole unimolecular decay pathway for isoprene-derived Criegee intermediates. *J. Phys. Chem. A* **124**, 3542–3554 (2020).

43. Lin, Y.-H., Yang, C.-H., Takahashi, K. & Lin, J. J.-M. Kinetics of unimolecular decay of methyl vinyl ketone oxide, an isoprene-derived Criegee intermediate, under atmospherically relevant conditions. *J. Phys. Chem. A* **124**, 9375–9381 (2020).

44. Anglada, J. M. & Solé, A. Impact of the water dimer on the atmospheric reactivity of carbonyl oxides. *Phys. Chem. Chem. Phys.* **18**, 17698–17712 (2016).

45. Spietz, P., Gómez Martín, J. C. & Burrows, J. P. Spectroscopic studies of the I_2/O_3 photochemistry: Part 2. Improved spectra of iodine oxides and analysis of the IO absorption spectrum. *J. Photochem. Photobiol. A* **176**, 50–67 (2005).

46. Sander, S. P. et al. *Chemical Kinetics and Photochemical Data for Use in Atmospheric Studies. Evaluation Number 17.* JPL Publication 10-6 (Jet Propulsion Laboratory, Pasadena, 2011).

47. Ting, W.-L., Chen, Y.-H., Chao, W., Smith, M. C. & Lin, J. J.-M. The UV absorption spectrum of the simplest Criegee intermediate CH_2OO. *Phys. Chem. Chem. Phys.* **16**, 10438–10443 (2014).

48. Foreman, E. S. et al. High resolution absolute absorption cross sections of the $\tilde{B}1A'$–$\tilde{B}1A'$ transition of the CH_2OO biradical. *Phys. Chem. Chem. Phys.* **17**, 32539–32546 (2015).

49. Lewis, T. R., Blitz, M. A., Heard, D. E. & Seakins, P. W. Direct evidence for a substantive reaction between the Criegee intermediate, CH_2OO, and the water vapour dimer. *Phys. Chem. Chem. Phys.* **17**, 4859–4863 (2015).

50. Smith, M. C. et al. UV absorption spectrum of the C2 Criegee intermediate CH_3CHOO. *J. Chem. Phys.* **141**, 074302 (2014).

51. Huang, H.-L., Chao, W. & Lin, J. J.-M. Kinetics of a Criegee intermediate that would survive high humidity and may oxidize atmospheric SO_2. *Proc. Nat. Acad. Sci. USA* **112**, 10857–10862 (2015).

52. Chhantyal-Pun, R., Davey, A., Shallcross, D. E., Percival, C. J. & Orr-Ewing, A. J. A kinetic study of the CH_2OO Criegee intermediate self-reaction, reaction with SO_2 and unimolecular reaction using cavity ring-down spectroscopy. *Phys. Chem. Chem. Phys.* **17**, 3617–3626 (2015).

53. Anglada, J. M. et al. Atmospheric significance of water clusters and ozone–water complexes. *J. Phys. Chem. A* **117**, 10381–10396 (2013).

54. Yin, C. & Takahashi, K. Effect of unsaturated substituents in the reaction of Criegee intermediates with water vapor. *Phys. Chem. Chem. Phys.* **20**, 20217–20227 (2018).

55. Pople, J. A., Head-Gordon, M. & Raghavachari, K. Quadratic configuration interaction. A general technique for determining electron correlation energies. *J. Chem. Phys.* **87**, 5968–5975 (1987).

56. Dunning, T. H. Gaussian basis sets for use in correlated molecular calculations. I. The atoms boron through neon and hydrogen. *J. Chem. Phys.* **90**, 1007–1023 (1989).

57. Peterson, K. A., Woon, D. E. & Dunning, T. H. Benchmark calculations with correlated molecular wave functions. IV. The classical barrier height of the $H+H_2 \rightarrow H_2+H$ reaction. *J. Chem. Phys.* **100**, 7410–7415 (1994).

58. Becke, A. D. Density-functional thermochemistry. III. The rol e of exact exchange. *J. Chem. Phys.* **98**, 5648–5652 (1993).

59. Lee, C., Yang, W. & Parr, R. G. Development of the Colle–Salvetti correlation-energy formula into a functional of the electron density. *Phys. Rev. B* **37**, 785–789 (1988).

60. Krishnan, R., Binkley, J. S., Seeger, R. & Pople, J. A. Self-consistent molecular orbital methods. XX. A basis set for correlated wave functions. *J. Chem. Phys.* **72**, 650–654 (1980).

61. Newland, M. J. et al. Atmospheric isoprene ozonolysis: impacts of stabilised Criegee intermediate reactions with SO_2, H_2O and dimethyl sulfide. *Atmos. Chem. Phys.* **15**, 9521–9536 (2015).

62. Nguyen, T. L., Lee, H., Matthews, D. A., McCarthy, M. C. & Stanton, J. F. Stabilization of the simplest Criegee intermediate from the reaction between ozone and ethylene: a high-level quantum chemical and kinetic analysis of ozonolysis. *J. Phys. Chem. A* **119**, 5524–5533 (2015).

63. Kuo, M.-T., Takahashi, K. & Lin, J. J.-M. Reactions of Criegee intermediates are enhanced by hydrogen-atom relay through molecular design. *Chem. Phys. Chem.* **21**, 2056–2059 (2020).

64. Li, Y.-L., Lin, C.-Y., Lin, Y.-H. & Lin, J. J.-M. Temperature-dependent kinetics of the simplest Criegee intermediate reaction with dimethyl sulfoxide. *J. Chin. Chem. Soc.* **67**, 1563–1570 (2020).

Acknowledgements

Author contributions

J.J.-M.L. conceived the experiment. Y.-H.L. set up the experiment, performed the measurements, and analyzed the experimental data. C.Y. and K.T. performed the theoretical calculations. Y.-H.L., C.Y., K.T. and J.J.-M.L. discussed the results. J.J.-M.L. wrote the paper.

Competing interests

The authors declare no competing interests.

Additional information